Multiple k magnetic structure and Fermi surface of USb

K. Knöpfle and L. M. Sandratskii
Institut für Festkörperphysik, Technische Universität, D-64289 Darmstadt, Germany
(Received 26 June 2000; published 11 December 2000)

We present calculations of the multiple **k** magnetic structures in USb in the framework of spin density functional theory. The system is described by a fully relativistic Hamiltonian including an orbital polarization correction term. Calculations are carried out with the modified augmented spherical waves method which takes into account the full-shape potential and the noncollinearity of the magnetization inside the atomic spheres. The experimentally determined evolution from the ground state triple-**k** structure towards the single-**k** structure under pressure is studied. The Fermi surface properties of the ground state triple-**k** structure are analyzed in detail and compared with experimental data.

DOI: 10.1103/PhysRevB.63.014411 PACS number(s): 75.10.Lp, 75.25.+z, 71.18.+y

I. INTRODUCTION

The complex noncollinear triple-**k** magnetic structure (Fig. 1) distinguishes USb from other compounds of the series of the uranium monopnictides UX (X=N, P, AS, Sb, and Bi).[1,2] Under pressure there is a phase transition into a single-**k** structure[3,4] (Fig. 1), which is a collinear antiferromagnetic structure formed by ferromagnetic planes with alternating directions of the atomic moments.

In contrast to the first three compounds in the series, UN, UP, and UAs, the experimental specific heat coefficient γ in USb is small.[5] The Sommerfeld coefficient increases constantly from 25.8 mJ/K^2 in UN to 53.2 mJ/K^2 in UA's but decreases in USb to 4.56 mJ/K^2. As this electronic specific heat is directly related to the density of electron states at the Fermi level, semimetal properties can be expected in the case of USb. This is experimentally confirmed by electrical resistivity measurements.[6] A small density of states at the Fermi level signals that only few bands cross the Fermi level and only few Fermi surface sheets are present.

The first density functional theory calculation of the multi-**k** structures in USb[7] reproduced the triple-**k** ground state and low Sommerfeld constant. In the present paper we extend the study of the electronic properties of USb and calculate the single- and triple-**k** structures at different lattice constants confirming the experimentally observed transition from triple- into single-**k** structure under pressure. We perform a detailed study of the Fermi surface properties of the triple-**k** structure and compare our theoretical results with experimental de Haas–van Alphen data.[8]

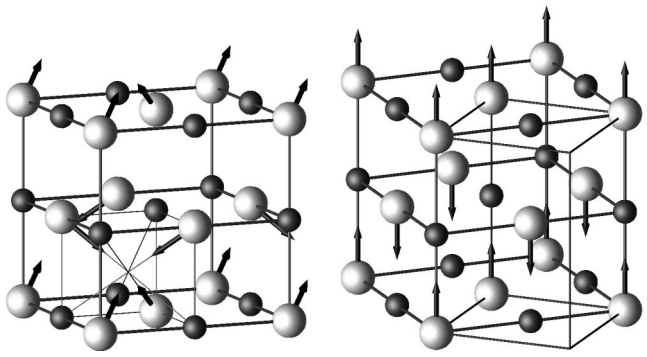

FIG. 1. Triple-**k** structure (left) and single-**k** structure (right) in USb.

II. CALCULATIONAL APPROACH

The calculations are carried out with the modified augmented spherical wave (MASW) method. The MASW method takes into account the full-shape potential inside the atomic spheres, which is expanded in spherical harmonics up to $l=8$. Besides, the variation of the direction of the magnetization inside the atomic spheres is taken into account. A detailed description of the MASW method is given elsewhere.[9] A number of calculational schemes which take into account the noncollinearity of the intra-atomic magnetization appeared in the last few years.[10–12] Because of the calculational complexity of this approach, very few studies of complex systems have been reported.

The fully relativistic Hamiltonian describing the system is written as a sum of four contributions

$$\hat{\mathbf{H}}=\hat{\mathbf{H}}_{\mathrm{sc}}+\hat{\mathbf{H}}_{\mathrm{so}}+\hat{\mathbf{H}}_{\mathrm{op}}+\hat{\mathbf{H}}_{\mathrm{nmt}}. \tag{1}$$

The first term $\hat{\mathbf{H}}_{\mathrm{sc}}$ is the scalar-relativistic Hamiltonian allowing for interatomic noncollinear magnetic structures[13]

$$\hat{\mathbf{H}}_{\mathrm{sc}}=\sum_{\nu}\mathbf{U}_{\nu}^{\dagger}\begin{pmatrix} H_{\mathrm{sc}}^{\nu\uparrow} & 0 \\ 0 & H_{\mathrm{sc}}^{\nu\downarrow}\end{pmatrix}\mathbf{U}_{\nu}. \tag{2}$$

Here the $\mathbf{U}_{\nu}=\mathbf{U}(\theta_{\nu},\phi_{\nu})$ are the spin-$\frac{1}{2}$ rotation matrices transforming into the local coordinate system of atom ν. The diagonal elements $H_{\mathrm{sc}}^{\nu\uparrow/\downarrow}$ are the standard scalar-relativistic Hamiltonians[14] for spin up and down in the νth atoms local frame. They are spherically averaged and contain the mass velocity and the Darwin term.

The second term $\hat{\mathbf{H}}_{\mathrm{so}}$ in Eq. (1) takes into account spin-orbit coupling. It can be written as

$$\hat{\mathbf{H}}_{\mathrm{so}}=\sum_{\nu}\mathbf{U}_{\nu}^{\dagger}\sum_{i=x,y,z}\{M_i^{\nu}\boldsymbol{\sigma}_i\hat{l}_i^{\nu}\}\mathbf{U}_{\nu}. \tag{3}$$

 ©2000 The American Physical Society

Here the $\boldsymbol{\sigma}_i$ are the Pauli spin matrices, $\hat{\boldsymbol{l}}^\nu$ is the angular momentum operator of the νth atom, and the coefficients M_i^ν can be found in Ref. 15.

The third term $\hat{\mathbf{H}}_{\rm op}$ in Eq. (1) is the orbital polarization correction (OPC) term. Following the work of Eriksson, Johansson, and Brooks[16] this term is written

$$\hat{\mathbf{H}}_{\rm op}=\sum_\nu I^\nu_{\rm orb} L_z^\nu \hat{l}_z^\nu \mathbf{1}. \tag{4}$$

Here the parameter $I^\nu_{\rm orb}$ is taken to be 2.6 mRyd for the U atoms as suggested in Ref. 16. L_z^ν is the projection of the orbital moment on the local z axis of atom ν and **1** is the 2×2 unity matrix.

The fourth term $\hat{\mathbf{H}}_{\rm nmt}$ in Eq. (1) includes all nonspherical and off-diagonal parts of the potential in the atomic sphere, not yet included in the first three terms. It can be written as

$$\hat{\mathbf{H}}_{\rm nmt}=\sum_\nu \mathbf{U}_\nu^\dagger \left[\begin{pmatrix} 0 & v_{00}^{\uparrow\downarrow}(r_\nu) \\ v_{00}^{\downarrow\uparrow}(r_\nu) & 0 \end{pmatrix} Y_{00}(\hat{\mathbf{r}}_\nu) + \sum_{\substack{l,m \\ l\neq 0}} \mathbf{v}_{lm}(r_\nu) Y_{lm}(\hat{\mathbf{r}}_\nu) \right] \mathbf{U}_\nu \tag{5}$$

The off-diagonal part of the potential takes into account intra-atomic noncollinearity of the spin densities which is treated in a self-consistent way. Within the MASW method there is no approximation on the shape of the 2×2 potential inside the atomic spheres.

III. SYMMETRY OF THE CRYSTAL AND MAGNETIC STRUCTURE

The uranium monopnictides crystallize in the face centered NaCl structure. The size of the magnetic unit cell depends on the magnetic structure. The single-**k** structure has a body centered tetragonal magnetic unit cell (Fig. 1) with two chemical units per cell. The magnetic unit cell of the triple-**k** structure is a simple cubic and containes four chemical units (Fig. 1).

To simplify calculations and to study the stability of the calculated magnetic structures the symmetry analysis is essential. Symmetry operations of a magnetic crystal must leave invariant both the positions of the atoms and the magnetic structure. In the presence of spin-orbit coupling spin and space variables are coupled and therefor a space rotation C must be accompanied by an identical spin rotation (see e.g., Refs. 17 and 18). Due to the axial nature of the magnetic moment the space inversion I leaves magnetic moments invariant. The symmetry operations can be written in the form $\{\alpha_R|\mathbf{t}\}$, where α_R is a rotation or a rotation accompanied by the inversion and **t** is a space translation.

In addition, the $\{\alpha_R|\mathbf{t}\}$ operations can be accompanied by the time reversal Θ which can be represented as $\Theta=\boldsymbol{\sigma}_y K$. Here $\boldsymbol{\sigma}_y$ is a Pauli spin matrix and K is the operator of complex conjugation. The Θ operator reverses the direction of magnetic moments.

TABLE I. Symmetry operations for single- and triple-**k** structures in USb. Here $\mathbf{t}_x=(\frac{1}{2}00)$, $\mathbf{t}_y=(0\frac{1}{2}0)$, $\mathbf{t}_{xy}=(\frac{1}{2}\frac{1}{2}0)$, $\mathbf{t}=(\frac{1}{2}\frac{1}{2}\frac{1}{2})$ and so on.

	Symmetry operations $\{\alpha_R\|\mathbf{t}\}$			
single-**k**				
	$\{E\|0\}$	$\{C_{2x}\|0\}$	$\{C_{2y}\|0\}$	$\{C_{2z}\|0\}$
	$\{C_{2b}\|\mathbf{t}_x\}$	$\{C_{4z}^-\|\mathbf{t}_y\}$	$\{C_{4z}^+\|\mathbf{t}_x\}$	$\{C_{2a}\|\mathbf{t}_y\}$
	$\{I\|\mathbf{t}\}$	$\{\sigma_x\|\mathbf{t}_z\}$	$\{\sigma_y\|\mathbf{t}_z\}$	$\{\sigma_z\|\mathbf{t}_z\}$
	$\{\sigma_{db}\|\mathbf{t}_{yz}\}$	$\{S_{4z}^+\|\mathbf{t}_{xz}\}$	$\{S_{4z}^-\|\mathbf{t}_{yz}\}$	$\{\sigma_{da}\|\mathbf{t}_{xz}\}$
triple-**k**				
	$\{E\|0\}$	$\{C_{2x}\|0\}$	$\{C_{2y}\|0\}$	$\{C_{2z}\|0\}$
	$\{C_{31}^-\|0\}$	$\{C_{32}^-\|0\}$	$\{C_{33}^-\|0\}$	$\{C_{34}^-\|0\}$
	$\{C_{31}^+\|0\}$	$\{C_{34}^+\|0\}$	$\{C_{32}^+\|0\}$	$\{C_{33}^+\|0\}$
	$\Theta\{C_{2b}\|\mathbf{t}\}$	$\Theta\{C_{4z}^-\|\mathbf{t}\}$	$\Theta\{C_{4z}^+\|\mathbf{t}\}$	$\Theta\{C_{2a}\|\mathbf{t}\}$
	$\Theta\{C_{2e}\|\mathbf{t}\}$	$\Theta\{C_{2c}\|\mathbf{t}\}$	$\Theta\{C_{4y}^-\|\mathbf{t}\}$	$\Theta\{C_{4y}^+\|\mathbf{t}\}$
	$\Theta\{C_{2f}\|\mathbf{t}\}$	$\Theta\{C_{4x}^+\|\mathbf{t}\}$	$\Theta\{C_{2d}\|\mathbf{t}\}$	$\Theta\{C_{4x}^-\|\mathbf{t}\}$
	$\{I\|\mathbf{t}\}$	$\{\sigma_x\|\mathbf{t}\}$	$\{\sigma_y\|\mathbf{t}\}$	$\{\sigma_z\|\mathbf{t}\}$
	$\{S_{61}^+\|\mathbf{t}\}$	$\{S_{62}^+\|\mathbf{t}\}$	$\{S_{63}^+\|\mathbf{t}\}$	$\{S_{64}^+\|\mathbf{t}\}$
	$\{S_{61}^-\|\mathbf{t}\}$	$\{S_{64}^-\|\mathbf{t}\}$	$\{S_{62}^-\|\mathbf{t}\}$	$\{S_{63}^-\|\mathbf{t}\}$
	$\Theta\{\sigma_{db}\|0\}$	$\Theta\{S_{4z}^+\|0\}$	$\Theta\{S_{4z}^-\|0\}$	$\Theta\{\sigma_{da}\|0\}$
	$\Theta\{\sigma_{de}\|0\}$	$\Theta\{\sigma_{dc}\|0\}$	$\Theta\{S_{4y}^+\|0\}$	$\Theta\{S_{4y}^-\|0\}$
	$\Theta\{\sigma_{df}\|0\}$	$\Theta\{S_{4x}^-\|0\}$	$\Theta\{\sigma_{dd}\|0\}$	$\Theta\{S_{4x}^+\|0\}$

The symmetry operations for the single- and triple-**k** structures in USb are collected in Table I. For the single-**k** structure 16 operations of tetragonal symmetry and in the case of the triple-**k** structure all 48 cubic symmetry operations leave the magnetic crystal invariant. The notation of Bradley-Cracknell[19] is used for the operators, E is the identity operation, I the space inversion, C is a pure rotation, σ is a reflection, and S is a rotation reflection. Θ denotes the time reversal operator.

The analysis according to the symmetry criterion formulated in our previous publications (see Ref. 20 for review) shows that both structures are stable and can be the ground state of the system. Which of the two structers is realized depends on the complex balance of various interactions and cannot be predicted on the basis of the symmetry arguments. A direct DFT calculation of both structures is needed to reveal the structure with lower energy. These calculations are reported in Sec. IV.

IV. RESULTS

A. Magnetic ground state

The experimentally[1] determined ground state in USb is the triple-**k** structure with a Neel temperature of $T_N=213$ K. The experimental lattice constant is $a=11.6993a_0$ (a_0 is the Bohr radius)[2] and the magnetic moments of the U atoms are measured to be $2.85\mu_B$. Under pressure a transition towards a single-**k** structure is observed.[3,4]

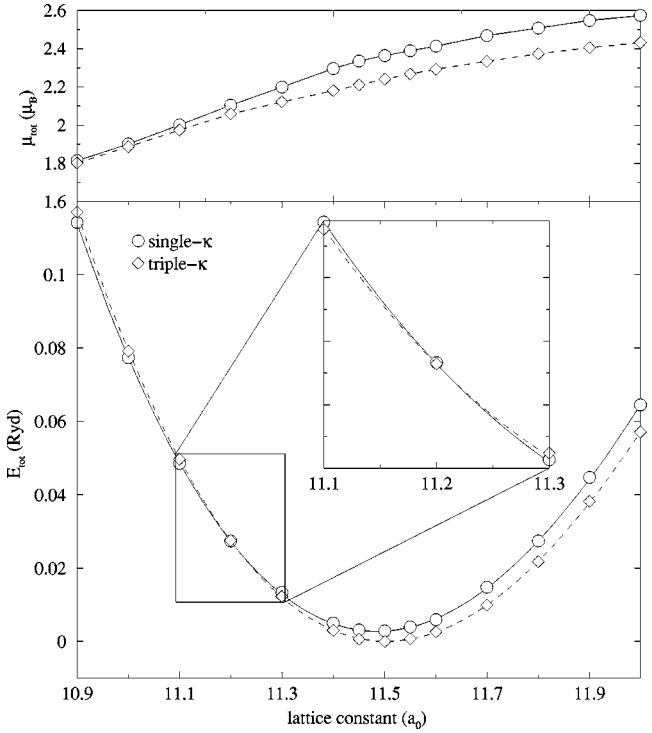

FIG. 2. Calculated total energy E_{tot} and magnetic moment for single- and triple-**k** structures in USb as a function of the lattice constant

We did a series of calculations for single- and triple-**k** structures for lattice constants of the cubic lattice varying from $a=10.9a_0$ to $a=12.0a_0$. The results are shown in Fig. 2.

As can be seen in Fig. 2, the calculated magnetic ground state is the triple-**k** structure with a lattice constant $a=11.5a_0$, in reasonable agreement with the experimental lattice constant. The calculated magnetic moment for the ground state is $2.24\mu_B$ which is the sum of an orbital moment of $4.46\mu_B$ and an oppositely directed spin moment of $2.22\mu_B$. Although the calculations fail to reproduce exactly the experimental value of the magnetic moment, this result is in much better agreement with experiment than the result of the earlier calculation[7] which gave a moment of $1.54\mu_B$. This improvement is mainly due to the OPC term, Eq. (4), which enhances the calculated orbital moments.

The transition from triple to single **k** is reproduced in the calculations. For lattice constants $a\leqslant 11.2a_0$ the single-**k** structure becomes energetically preferable. The magnetic moment of the single-**k** structure for $a=11.3a_0$ is $2.20\mu_B$ per U atom with an orbital moment of $4.26\mu_B$ and an oppositely directed spin moment of $2.06\mu_B$. The size of the moment decreases with decrease of the lattice constant (Fig. 2).

B. The Fermi surface in USb

Next we discuss the Fermi surface of the triple-**k** structure, calculated for the theoretical equilibrium lattice constant $a=11.5a_0$. Analysis of the band structure (Fig. 3) reveals that there are three bands crossing the Fermi level. The calculated density of states shows a small number of states at

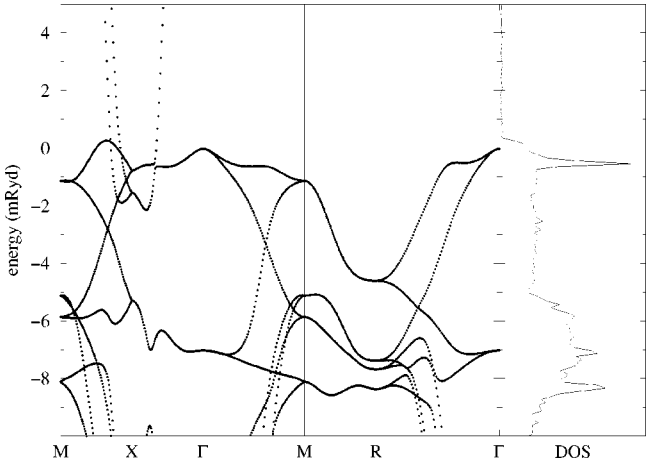

FIG. 3. Band structure (left) near the Fermi energy and the density of states (right) for the triple-**k** structure in USb.

the Fermi level. This property is in agreement with the small experimental Sommerfeld coefficient for USb.[5]

The three bands crossing the Fermi level result in three Fermi surface sheets. One encloses hole states; the other two enclose electron states. The Fermi surface sheets are shown in Figs. 4(a)–4(d). The first sheet [Fig. 4(a)] consists of rings centered around the *X* point. The second sheet [Fig. 4(b)] looks like dog bones centered at the *X* points while the third sheet [Fig. 4 (c)] looks like cigars.

The symmetry of the triple-**k** structure is reflected in the form of the Fermi surfaces. The fourfould rotations about the coordinate axes, the threefold rotations about the diagonals, and the reflections and rotation reflections collected in the Table I leave the Fermi surface invariant.

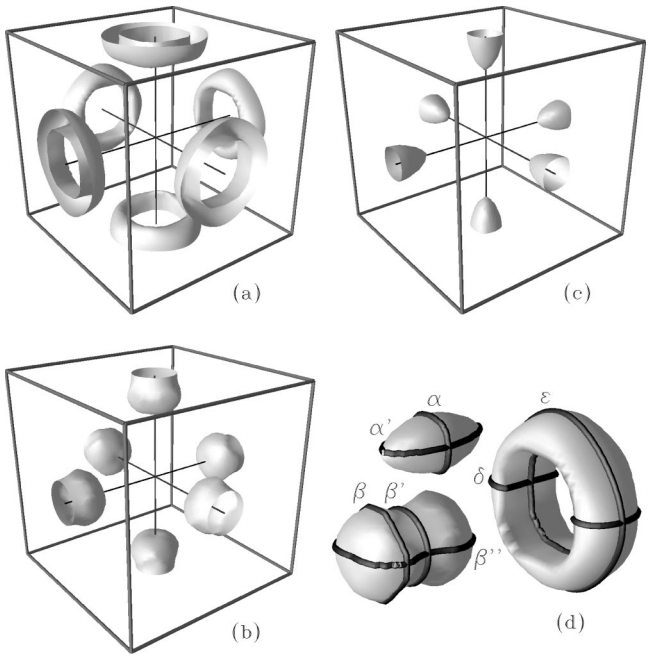

FIG. 4. Fermi surface sheets in triple-**k** USb. The first two sheets (a) and (b) enclose hole states, and the third sheet (c) encloses electron states.

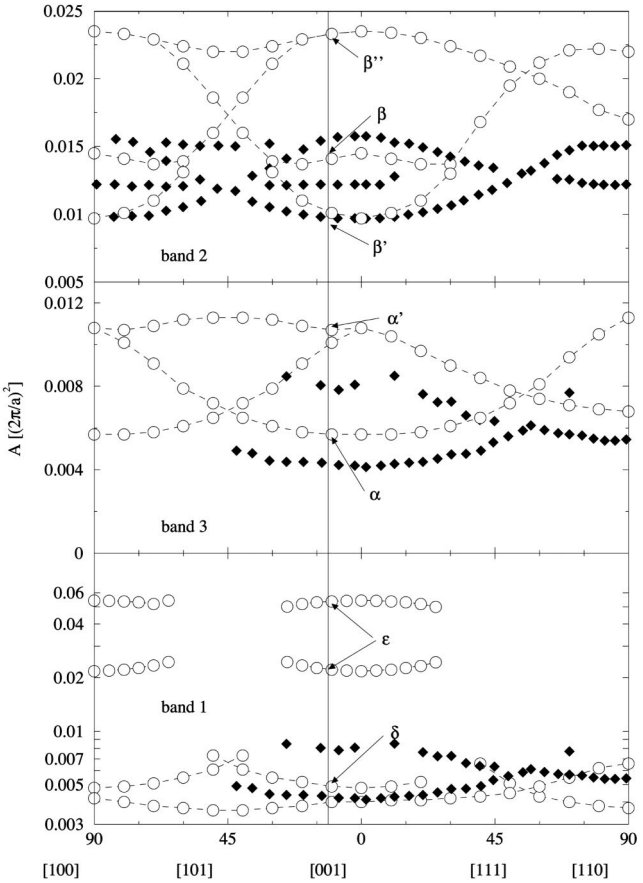

FIG. 5. Theoretical (○) and experimental (♦) de Haas–van Alphen data for triple-**k** USb. The greek letters indicate the extremal cross sections shown in Fig. 4(d).

In Fig. 4(d) the Fermi surface sheets are shown together with several extremal cross sections labeled with Greek letters. The cross sections α and β are labeled in the same way as in Ref. 8. The de Haas–van Alphen measurements suggested two cigar-like Fermi sheets at the X points and a spherical sheet at the Γ point. The two cigar shaped Fermi surface sheets are reproduced by our calculations, whereas no spherical sheet is found at the Γ point, although the upper occupied bands at the Γ point are very close to the Fermi level (see Fig. 3). The suggested spherical Fermi surface sheet could not be detected experimentally over the whole range of orientations of the applied magnetic field, although this is expected for a spherical sheet. On the other hand, there is no experimental evidence for the first theoretical Fermi surface sheet shown in Fig. 4(a).

The special form of the dog bone sheet suggests an explanation for the failure of the experiments to observe the suggested spherical Fermi sheet over the whole range of field direction. To show this, the experimental de Haas–van Alphen data are compared with the theoretical data in Fig. 5. The upper graph shows the data for the second theoretical sheet [Fig. 4(b)] and corresponding experimental data. Although there is no good quantitative agreement between theory and experiment the qualitative agreement is very good. The experimental data were interpreted as coming from; first, cigar shaped sheets at the X points which are responsible for the branches labeled with β and β'' and second, a spherical sheet at the Γ point leading to the constant frequency branch.

We suggest an alternative interpretation. The shape of the dog bone sheet leads to a separation of the extremal cross sections into a minimum β' and a maximum β cross section for field orientations near the (001) and (100) direction. For these field orientations the maximum cross section β is rather constant, whereas for field orientations far from Cartesian axes there is no cross sections of β type.

The de Haas–van Alphen data for the cigar shaped theoretical Fermi surface sheet is compared with the experimental data in the middle graph in Fig. 5. Here, the agreement between theoretical and experimental data is very good; the branches α and α' are reproduced in good quantitative agreement. For the first ring shaped theoretical sheet there is no clear experimental evidence. The theoretical de Haas–van Alphen data for this sheet are shown in the lower graph in Fig. 5. The large cross sections ϵ belonging to the inner and outer cross section of the ring are not seen experimentally. The smaller cross section δ may be represented by the lower branches of the experimental data. This is, however, the data we already assinged to the cigar shaped sheet.

V. CONCLUSIONS

We have studied single- and triple-**k** magnetic structures in USb by means of *ab initio* calculations in the framework of spin density functional theory. In agreement with the experiment we obtained the triple-**k** structure to be the magnetic ground state. Also the transition into a single-**k** ground state under pressure is successfully reproduced. The calculated magnetic moment of uranium atoms is in reasonable agreement with the large experimental moments.

A detailed analysis of the Fermi surface properties is performed. A comparison of the calulated extremal cross sections of the Fermi surface sheets with experimental de Haas–van Alphen data is given and a new interpretation of the experimental data is suggested. We hope the present theoretical work will stimulate further experimental and theoretical studies of the Fermi surface and electronic properties of this compound.

Our recent calculation of the double-**k** structure in USb for the experimental lattice parameter gave the total energy very close to the total energy of the triple-**k** configuration. Further studies are needed to understand the role of the double-**k** magnetic state.

ACKNOWLEDGMENTS

This work was supported by the Deutsche Forschungsgesellschaft (DFG) ''Schwerpunktprogramm relativistische Effekte.'' The authors are grateful to J. Kübler for comments on the manuscript.

[1] J. Rossat-Mignod, P. Burlet, S. Quezel, and O. Vogt, Physica B & C **102B**, 237 (1980).
[2] G.H. Lander and P. Burlet, Physica B **215**, 7 (1995).
[3] J.-M. Mignot, I.N. Goncharenko, D. Braithwaite, and O. Vogt, J. Phys. Soc. Jpn. **65**, 91 (1996).
[4] D. Braithwaite, I.N. Goncharenko, J.-M. Mignot, A. Ochiai, and O. Vogt, Europhys. Lett. **35**, 121 (1996).
[5] H. Rudigier, H.R. Ott, and O. Vogt, Phys. Rev. B **32**, 4584 (1985).
[6] J. Schoenes, B. Frick, and O. Vogt, Phys. Rev. B **30**, 6578 (1984).
[7] H. Yamagami, Phys. Rev. B **61**, 6246 (2000).
[8] A. Ishiguro, H. Aoki, O. Sugie, M. Suzuki, A. Sawada, N. Sato, T. Komatsubara, A. Ochiai, T. Suzuki, K. Suzuki, M. Higuchi, and A. Hasegawa, J. Phys. Soc. Jpn. **66**, 2764 (1997).
[9] K. Knöpfle, L. M. Sandratskii, and J. Kübler, Phys. Rev. B **62**, 5564 (2000).
[10] L. Nordström and D.J. Singh, Phys. Rev. Lett. **76**, 4420 (1996).
[11] T. Oda, A. Pasquarello, and R. Car, Phys. Rev. Lett. **80**, 3622 (1998).
[12] H. Eschrig and V.D.P. Servedio, J. Comput. Chem. **20**, 23 (1999).
[13] M. Uhl, L.M. Sandratskii, and J. Kübler, Phys. Rev. B **50**, 291 (1994).
[14] D.D. Koelling and B.N. Harmon, J. Phys. C **10**, 3107 (1977).
[15] L.M. Sandratskii, J. Kübler, P. Zahn, and I. Mertig, Phys. Rev. B **50**, 15 834 (1994).
[16] O. Eriksson, B. Johansson, and M.S.S. Brooks, J. Phys.: Condens. Matter **1**, 4005 (1989).
[17] L.M. Sandratskii, and J. Kübler, Physica B **217**, 167 (1996).
[18] L.M. Sandratskii, and J. Kübler, Phys. Rev. B **55**, 11 395 (1997).
[19] C. J. Bradley and A. P. Cracknell, *The Mathematical Theory of Symmetry in Solids* (Clarendon, Oxford, 1972).
[20] L.M. Sandratskii, Adv. Phys. **47**, 91 (1998).